Inorganic Chemistry

pubs.acs.org/IC

Article

Superconductivity in Crystallographically Disordered $LaHg_{6.4}$

Yurii Prots, Mitja Krnel, Yuri Grin, and Eteri Svanidze*

Cite This: *Inorg. Chem.* 2022, 61, 15444−15451

Read Online

ACCESS | Metrics & More | Article Recommendations | Supporting Information

ABSTRACT: The influence of structural disorder on superconductivity is not yet fully understood. A concurrent examination of crystallographic and physical properties of $LaHg_{6.4}$ reveals that this material enters a superconducting state below T_c = 2.4 K while showing crystallographic disorder in one dimension. Lanthanum mercuride, which crystallizes in a new structure type (space group *Cmcm*, a = 9.779(2) Å, b = 28.891(4) Å, c = 5.0012(8) Å, Z = 8), has remained out of reach for nearly 50 years. In this crystal structure, strong disorder is present in the channels that propagate along the [001] direction. By implementing a combination of cutting-edge synthesis and characterization techniques, we were able to circumvent the complexity associated with the low formation temperature and chemical reactivity of this substance and study the superconductivity of $LaHg_{6.4}$ in detail.

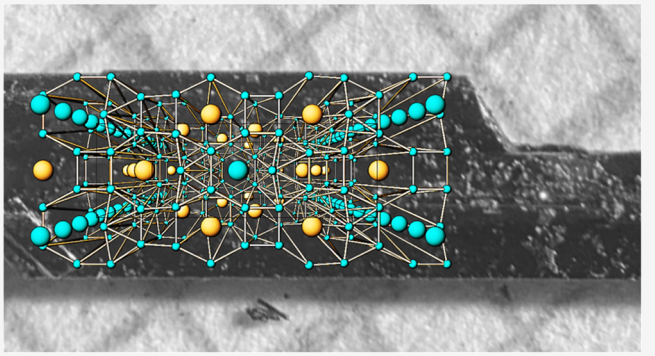

INTRODUCTION

It is well known that the chemical and physical properties of solid-state materials are deeply interrelated.[1−3] In particular, changes in the crystal lattice and the resultant structural disorder are frequently used as tuning parameters to change the ground state of a given material. Although typically, the lack of translational symmetry prohibits the appearance of superconductivity, the coexistence of the latter with structural disorder has been observed in some two- and three-dimensional materials.[4−11] For one-dimensional compounds, the effect of disorder on both bulk and topological superconductivity is not yet well-understood.[12−15]

Mercury-based compounds (amalgams) have received a considerable amount of attention in the chemical community—these materials often host complex crystallographic arrangements[16−27] and display peculiar bonding features.[22,28−34] As a result, some of these materials show peculiar superconducting characteristics,[21,32,35−47] including high critical temperatures, which can be enhanced even further by the application of pressure. Some mercury-containing materials were even suggested to exhibit topologically nontrivial states.[48−54] Moreover, peculiar magnetic correlations, brought on by the mixing of d and f orbitals, have been observed in several solid-state compounds.[23,51−60] Additionally, the application potential of some mercury-based materials has been discussed.[23,61] However, it is well-known that much care must be taken during the synthesis, handling, and characterization of mercury-based compounds, in particular rare earth metals' mercurides—from toxicity concerns to their high chemical reactivity—as these systems pose several experimental challenges.[27,62−64] The complexity of work on mercury-based materials is reflected in a low number of systems that have been discovered so far. Furthermore, detailed investigations of chemical and physical properties are often missing even for binary and ternary compounds that are already known. In the La−Hg system, the existence of $LaHg$,[17] $LaHg_2$,[17] $LaHg_3$,[65] $La_{11}Hg_{45}$,[64] $La_{13}Hg_{58}$,[65] and $LaHg_{6\sim}$[65] has been reported. However, an in-depth analysis of their properties remains to be carried out.

RESULTS AND DISCUSSION

The newly rediscovered lanthanum mercuride $LaHg_{6.4}$ is the most mercury-rich phase in the La−Hg system. While the first report regarding the existence of the "$LaHg_{6\sim}$" compound suggested orthorhombic crystal structure and lattice parameters in 1976,[65] the comprehensive structural characterization of $LaHg_{6.4}$ has been missing for nearly 50 years. This can be understood by the experiential difficulty of mercury-based materials—in addition to high X-ray absorption, the $LaHg_{6.4}$ compound is extremely air-sensitive, decomposing immediately even after a few second of air exposure. We have therefore prepared and characterized mm-sized single crystals of $LaHg_{6.4}$ (Figure 1) in a protective environment using several dedicated experimental techniques.

Received: June 9, 2022
Published: September 2, 2022

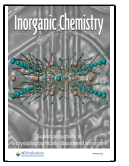

https://doi.org/10.1021/acs.inorgchem.2c01987
Inorg. Chem. 2022, 61, 15444−15451

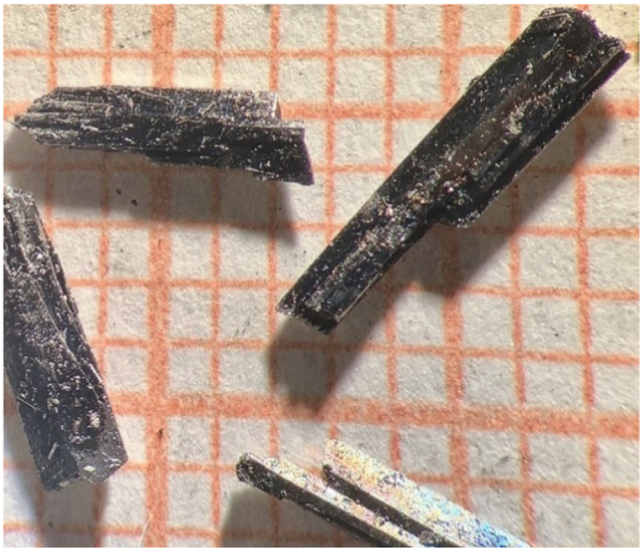

Figure 1. Single crystals of $LaHg_{6.4}$. Minute exposure to air results in an immediate degradation of the sample, as evidenced by the rough surface of the single crystals and microscopic mercury droplets, appearing on their surface. The smallest squares have a dimension of 1 mm × 1 mm.

The crystal structure was conclusively established based on the single-crystal X-ray diffraction experiment (see Tables S1–S3 for the corresponding crystallographic information). The diffraction data were indexed using orthorhombic lattice parameters a = 9.779(2) Å, b = 28.891(4) Å, and c = 5.0012(8) Å (close to those reported earlier[65]), and the extinction conditions agreed well with the C-centered lattice indicated in ref 65. Application of charge-flipping techniques allowed to determine the basic atomic arrangement (Figure 2, top), implying enlarged atomic displacement parameters for selected mercury atoms (Hg5, Hg7) and channels within the mercury sublattice formed by Hg2, Hg6, and Hg7 and running along the [001] direction with the main axes [00z] and [$^1/_2$ $^1/_2$ z]. Calculation of residual electron density with only La and Hg atoms of the basic atomic arrangement reveals quasi-continuous density distribution along the channels' axes (Figure 2, middle). For its appropriate description, additional partially occupied mercury positions were used (Hg10, Hg11). The atomic chain that fills up the channel is obviously incommensurate with respect to the remaining structure. Moreover, due to the large distance between the channels, their occupation seems to not be synchronized. This leads to the disorder around the Hg5 and Hg7 atoms, located at the channels' walls, and split positions have to be used to describe the local order in this region. While the split position Hg5 is completely occupied, the sum of occupancies of the Hg7, Hg8, and Hg9 positions is not unity, i.e., the noncommensurable occupation of the channels causes "breathing" within the channel wall at some places. Further signs of local violations of the translational symmetry can be recognized in the strong anisotropy of the atomic displacement of the Hg6 and La1 positions, which are located in the surrounding of the channels. This results in deviations from the previously suggested 1:6 stoichiometry,[65] yielding composition $LaHg_{6.4}$, i.e., $LaHg_{6-x+y}$. Partial incommensurability can sometimes be described by means of modulations. In the case of $LaHg_{6.4}$, no satellite reflections were observed in the single-crystal X-ray diffraction experiments. Thus, the establishment of the modulation vector was not possible.

The majority of the Hg–Hg distances vary as 2.88 Å ≤ d_{Hg-Hg} ≤ 3.39 Å, similar to what is observed in elemental Hg with d_{Hg-Hg} = 2.99–3.46 Å.[73] A comparison of the latter values with the lattice parameter c = 5.0012(8) Å of $LaHg_{6.4}$ indicates that it is not possible to localize 2 Hg species along this direction within one lattice parameter, as required by the symmetry of the space group *Cmcm* or its noncentrosymmetric variants. Thus, local symmetry breaking is present. Attempts to refine the data using noncentrosymmetric groups did not yield lower residual factors and did not allow to model ordering in the channels.

Interestingly, the short lanthanum–lanthanum contacts appear to be absent, with the shortest d_{La-La} = 4.93 Å being rather large. In comparison, those observed in elemental lanthanum are d_{La-La} ∼ 3.76 Å. For the lanthanum atoms, two crystallographic positions exist: La1 is coordinated by 14 Hg atoms in the form of a bicapped hexagonal prism, while La2 is coordinated by 13 Hg atoms. The coordination of La2 can be described as a modified cuboctahedron, where one of the apexes (Hg) is replaced by two Hg atoms. For a polyhedral representation of the structure, see Figures 1 and 4 in ref 66. In comparison, in mercury-poorer $La_{11}Hg_{45}$, lanthanum atoms have regular cuboctahedra as coordination polyhedra.[16]

The first indication of superconductivity in $LaHg_{6.4}$ is given by a sharp diamagnetic transition at T_c = 2.4 K (Figure 3a), observed in zero-field-cooled magnetic susceptibility data. Given that the superconducting volume fraction is over 100%, magnetization data indicate bulk superconductivity of the studied sample, which is further confirmed by specific heat and resistivity data, shown below. The crystals of $LaHg_{6.4}$, which have a rectangular rod-like morphology (see Figure 1), were oriented with the c-axis, i.e., the longer side of the crystal, parallel to the direction of the applied magnetic field. A slight enhancement of the Meissner fraction above the value of 1 can be explained by microscopic inclusions of Hg in the $LaHg_{6.4}$ crystals. The shape of magnetic isotherms (Figure 3b) is consistent with type-II superconductivity in this compound. The presence of residual mercury[67,68] on the surface as well as inside the $LaHg_{6.4}$ crystals is also evident from the secondary transitions, observed in the temperature- and field-dependent magnetization data around T = 4 K (Figure 3a) and H = 30 mT (Figure 3b), respectively. The bulk superconductivity of the $LaHg_{6.4}$ compound is confirmed by the anomaly in the specific heat data, as shown in Figure 3c. The value of the electronic specific heat coefficient γ = 4.8 mJ $mol_{F.U.}^{-1}$ K^{-2}, while the size of the specific heat jump $\Delta C_e/\gamma_n T_c$ = 0.75 is significantly less than the expected BCS value ($\Delta C_e/\gamma_n T_c$ = 1.43). The latter can likely be attributed to the difficulties of background subtraction for samples with a small mass (see Materials and Methods section for further details). The Debye temperature θ_D = 424 K is used to estimate the magnitude of the electron–phonon coupling λ_{e-p} = 0.43, consistent with the conventional superconductivity of $LaHg_{6.4}$.

The superconductivity of $LaHg_{6.4}$ can be gradually suppressed by the application of a magnetic field, as observed from magnetization, specific heat, and resistivity data. The resultant H–T phase diagram (Figure 3e) is typical of that of a type-II superconductor. The superconducting state is observed below T_c and lower critical field $H_{c1}(0)$ = 25 mT. The region between the superconducting and normal states, also known as the mixed state, occurs below T_c and $H_{c2}(0)$ = 61 mT. The

https://doi.org/10.1021/acs.inorgchem.2c01987
Inorg. Chem. 2022, 61, 15444–15451

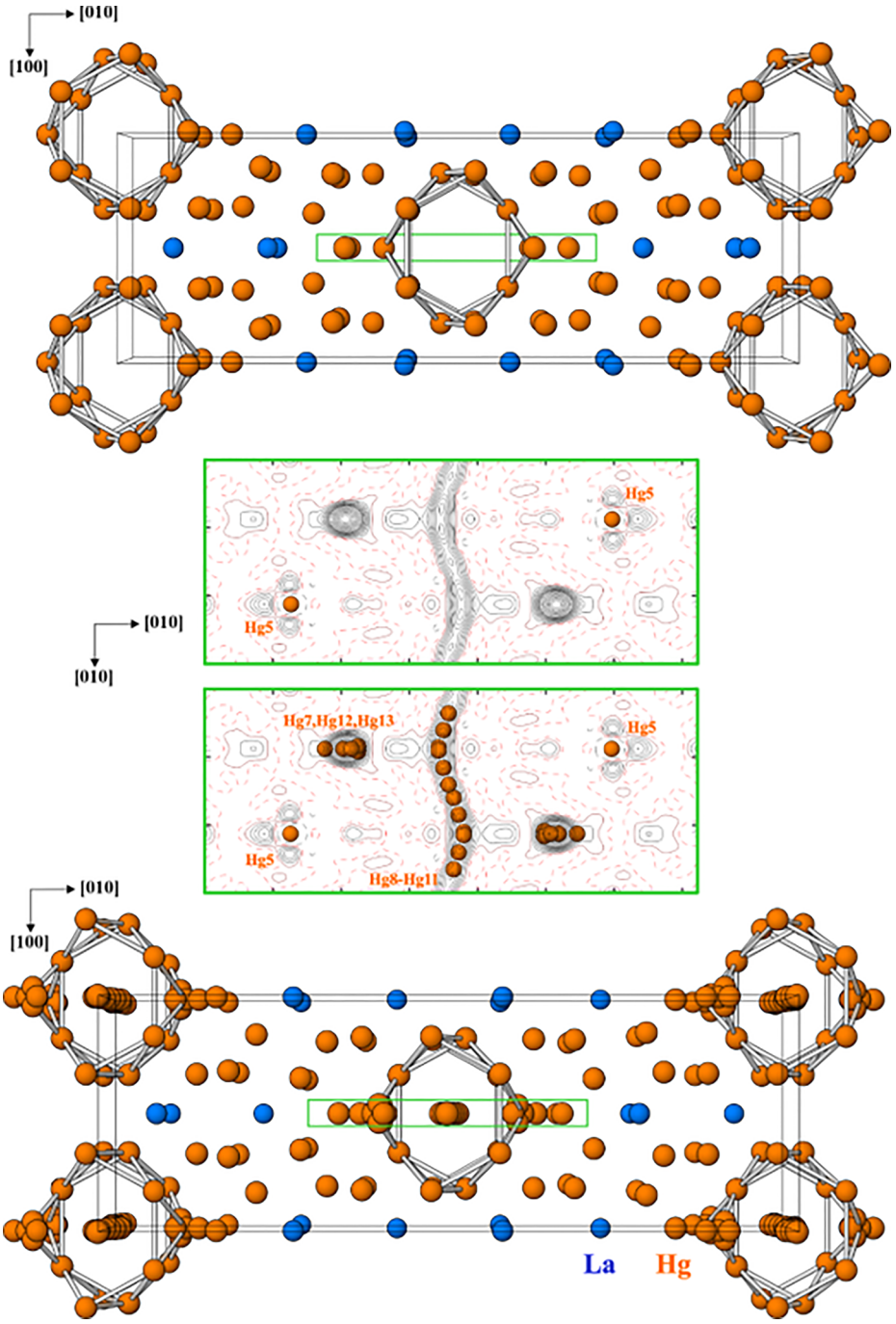

Figure 2. Crystal structure of $LaHg_{6.4}$: (top) basic atomic arrangement with channels running along the [001] direction with the main axes [00z] and [$^1/_2$ $^1/_2$ z]; (middle) distribution of the difference electron density within and around the channels (green region in the top and bottom panels) with mercury split positions used for its description; and (bottom) a perspective view of the complete crystal structure along [001].

Ginzburg–Landau parameter $\kappa(0) = 3.2 > 1/\sqrt{2}$ is in agreement with $LaHg_{6.4}$ being a type-II superconductor.

CONCLUSIONS

In this work, we present the discovery and characterization of $LaHg_{6.4}$—a quasi-one-dimensional (1D) crystallographically disordered compound that enters the superconducting state below T_c = 2.4 K. This material has remained out of reach for nearly 50 years, as a result of experimental challenges of the work on mercury-containing compounds (amalgams). Using a number of cutting-edge synthesis and characterization tools, we were able to synthesize mm-sized single crystals of $LaHg_{6.4}$, which shows bulk superconductivity below T_c = 2.4 K. Further investigations of the electronic structure of $LaHg_{6.4}$ and isotypic phases are expected to shed more light on the relation between dimensionality and disorder in this peculiar material.

MATERIALS AND METHODS

All sample preparation and handling were performed in a specialized laboratory, equipped with an argon-filled glovebox system (MBraun, $p(H_2O/O_2)$ < 0.1 ppm).[69] Single crystals of $LaHg_{6.4}$ were synthesized from La (pieces, Ames Laboratory, >99.9%) and Hg (ChemPur, 99.999%) using the self-flux method. The La chunks and Hg droplets, mixed in the 5:95 ratio, were sealed in Ta tubes under an Ar

https://doi.org/10.1021/acs.inorgchem.2c01987
Inorg. Chem. 2022, 61, 15444−15451

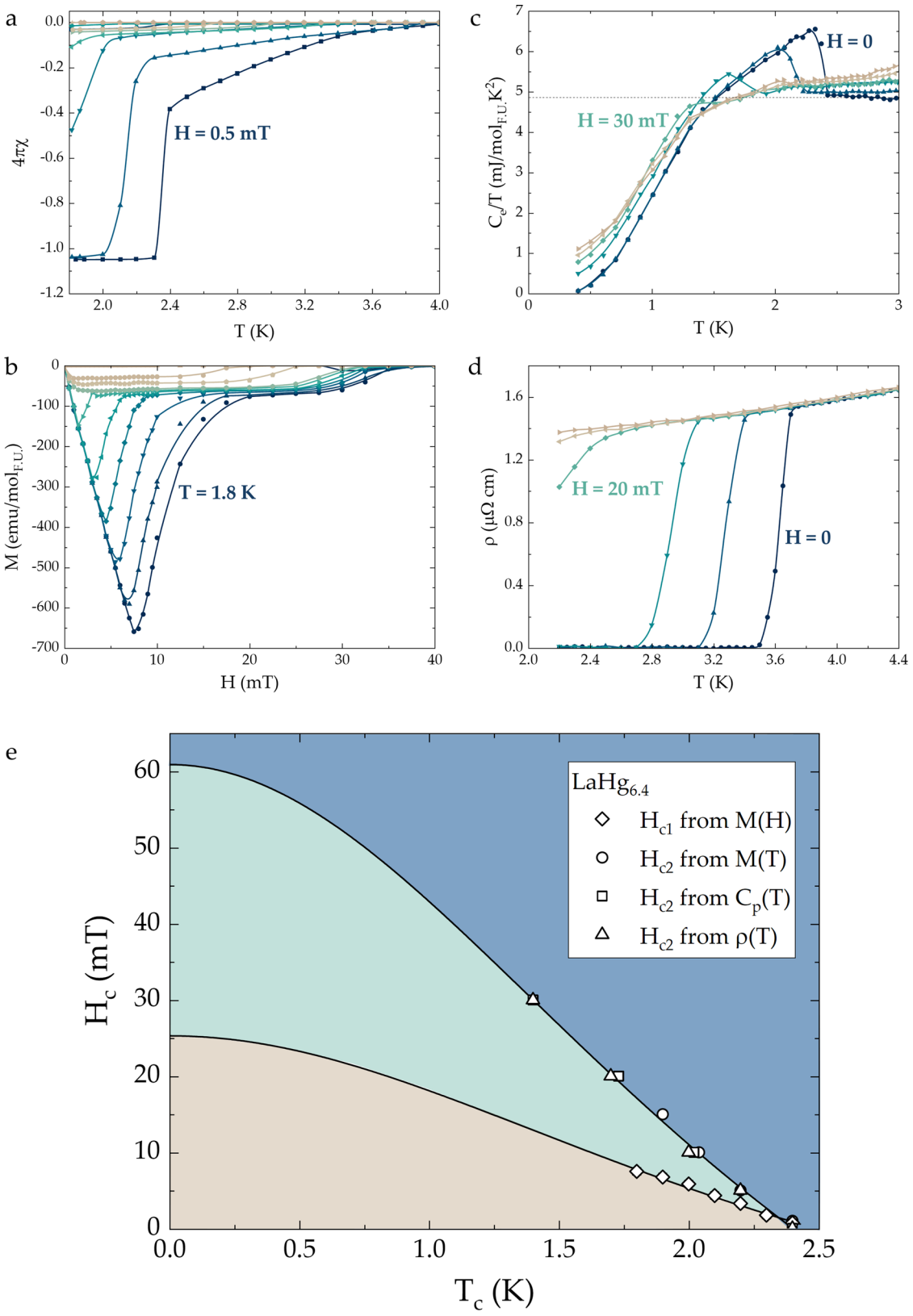

Figure 3. Superconducting properties of $LaHg_{6.4}$. Magnetization as a function of (a) temperature and (b) magnetic field. Temperature-dependent (c) specific heat and (d) resistivity data in various applied magnetic fields. (e) The phase diagram for $LaHg_{6.4}$ has three regions typical for a type-II superconductor.

atmosphere (Figure S1a,b). The volume of the Ta tubes, chosen so as to exclude Hg loss, was ~2 cm^3 for a total sample mass of 1 g. The sealed Ta tubes were heated to 500 °C and then slowly cooled to room temperature over a period of 10 days. Excess Hg flux was decanted at room temperature via centrifugation in custom-made crucibles shown in Figure S1b. Residual mercury could not be

https://doi.org/10.1021/acs.inorgchem.2c01987
Inorg. Chem. 2022, 61, 15444−15451

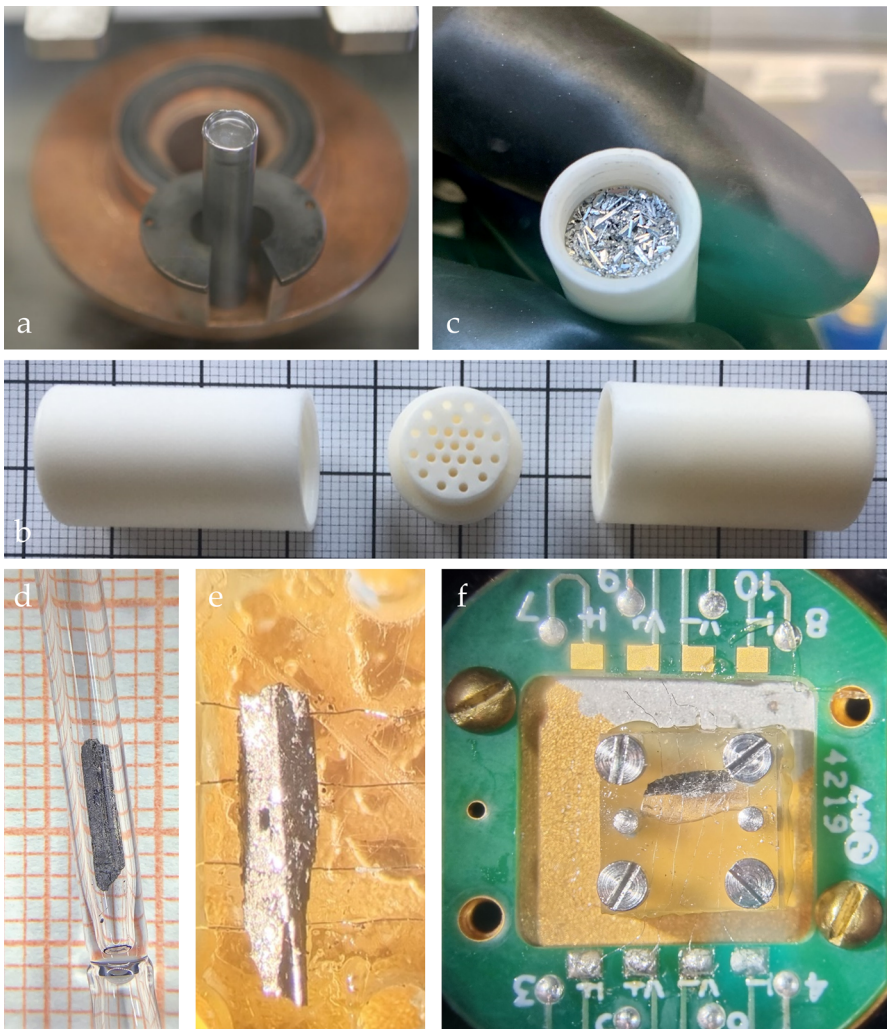

Figure 4. Synthesis and characterization of $LaHg_{6.4}$. (a) Sealed Ta ampoules contain custom-made alumina crucibles, shown in (b). (c) The residual mercury is easily decanted. The resultant crystals have needle- or slab-like morphology. (d) To protect samples from oxidation, single crystals are sealed under argon inside a quartz capillary. (e, f) A cell designed for measuring the resistivity of air-sensitive samples—wires are held in place by a Plexiglas platform, and the sample is surrounded by vacuum grease.

completely removed from the surface of the crystals. The resultant crystals had silver luster and needle- or slab-like morphology, with some examples shown in Figure S1c. Despite strong crystallographic disorder, the value of the residual resistivity ratio is rather large, RRR = 63. Similar to the other mercury-based binary compounds,[19,57,70] the $LaHg_{6.4}$ phase exhibited extreme air and moisture sensitivity, resulting in immediate decomposition even after a few seconds of exposure to air. Additionally, the $LaHg_{6.4}$ crystals were rather fragile, breaking easily when touched by tweezers.

Powder X-ray diffraction was performed on a Huber G670 Image plate Guinier camera with a Ge monochromator ($CuK\alpha_1$, λ = 1.54056 Å). Phase identification was done using WinXPow software.[71] The lattice parameters were determined by a least-squares refinement using the peak positions, extracted by profile fitting (WinCSD software[72]). Small single crystals with a size of ∼50 μm were suitable for single-crystal diffraction experiments. Single-crystal diffraction data were collected using a Rigaku AFC7 diffractometer, equipped with a Saturn 724+ CCD detector and a $MoK\alpha$ radiation source (λ = 0.71073 Å). WinCSD software[72] was used for crystallographic calculations. The crystallographic information is provided in Tables S1−S3.

The magnetic properties were studied using a Quantum Design (QD) Magnetic Property Measurement System for the temperature range from T = 1.8 to 300 K and for applied magnetic fields up to H = 7 T. Individual crystals were sealed inside glass tubes, both to protect the sample from oxidation and to ensure sample orientation, with an example shown in Figure 4d. Temperature- and field-dependent magnetization measurements were performed with a magnetic field applied parallel to the c-axis, eliminating the need for demagnetization correction. The Meissner fraction was determined from zero-field-cooled data as $4\pi\chi$, using the calculated density of $LaHg_{6.4}$ of 13.44 g cm^{-3}. The value of the Meissner fraction exceeding 1 can be attributed to either (i) excess elemental mercury inside or on the surface of the crystals or (ii) deviations of the sample shape from the ideal cylinder geometry. The former is supported by the observation of a feature associated with the freezing of elemental mercury in the temperature-dependent resistivity data (see Figure S1). The values of H_{c1} were extracted from magnetic isotherms, shown in Figure 3b, as the field at which the $M(H)$ curves deviate from the line with the initial slope of the $M(H)$ curve. The values of H_{c2} were extracted from temperature-dependent magnetization, specific heat, and resistivity data. For the latter, a constant temperature offset was used to account for the poor thermal coupling of the sample and the platform (see below).

The specific heat data were collected on a QD Physical Property Measurement System (PPMS) in the temperature range from T = 0.4 to 10 K for magnetic fields up to H = 9 T. Given the high air sensitivity of the $LaHg_{6.4}$ crystals, a large amount of grease was used to protect the sample. This, together with the small size of the signal produced by the $LaHg_{6.4}$ crystal, can sometimes lead to a large

https://doi.org/10.1021/acs.inorgchem.2c01987
Inorg. Chem. 2022, 61, 15444−15451

background contribution to the specific heat. As a result, it is possible that the magnitude of the specific heat jump is underestimated.

For resistivity measurements, it was noticed that silver paint or glues react with the surface of the $LaHg_{6.4}$ crystals, producing a thin layer of mercury. In this case, the resistivity measurements are dominated by the properties of mercury. To address this challenge, a special cell was designed—see Figure 4e,f. The handling of the cell was done inside a glovebox. The cell is composed of two sheets of Plexiglas, held together by screws, with platinum wires pressed on top of the sample. A layer of grease was used to protect the sample from oxidation. The superconducting transition observed in resistivity was offset by approximately 1 K from that observed in magnetization and specific heat data. This can either be attributed to (i) the thermal lag in coupling between the sample and the platform or (ii) the pressure effect, induced by the plates. The inherent reason behind this discrepancy is still being investigated.

■ ASSOCIATED CONTENT

Supporting Information

The Supporting Information is available free of charge at https://pubs.acs.org/doi/10.1021/acs.inorgchem.2c01987.

Crystallographic data, together with electrical resistivity measurements (PDF)

Accession Codes

CCDC 2178690 contains the supplementary crystallographic data for this paper. These data can be obtained free of charge via www.ccdc.cam.ac.uk/data_request/cif, or by emailing data_request@ccdc.cam.ac.uk, or by contacting The Cambridge Crystallographic Data Centre, 12 Union Road, Cambridge CB2 1EZ, UK; fax: +44 1223 336033.

■ AUTHOR INFORMATION

Corresponding Author

Eteri Svanidze − *Max-Planck-Institut für Chemische Physik fester Stoffe, Dresden 01187, Germany;* orcid.org/0000-0003-2893-1379; Email: svanidze@cpfs.mpg.de

Authors

Yurii Prots − *Max-Planck-Institut für Chemische Physik fester Stoffe, Dresden 01187, Germany;* orcid.org/0000-0002-7418-9892

Mitja Krnel − *Max-Planck-Institut für Chemische Physik fester Stoffe, Dresden 01187, Germany*

Yuri Grin − *Max-Planck-Institut für Chemische Physik fester Stoffe, Dresden 01187, Germany;* orcid.org/0000-0003-3891-9584

Complete contact information is available at: https://pubs.acs.org/10.1021/acs.inorgchem.2c01987

Funding

Open access funded by Max Planck Society.

Notes

The authors declare no competing financial interest.

■ ACKNOWLEDGMENTS

E.S. is grateful for the support of the Christiane Nüsslein-Volhard-Stiftung.

■ REFERENCES

(1) Gui, X.; Lv, B.; Xie, W. Chemistry in Superconductors. *Chem. Rev.* **2021**, *121*, 2966−2991.

(2) Goldman, A. M.; Marković, N. Superconductor-insulator transitions in the two-dimensional limit. *Phys. Today* **1998**, *51*, 39−44.

(3) Anderson, P. W. Theory of dirty superconductors. *J. Phys. Chem. Solids* **1959**, *11*, 26−30.

(4) Brun, C.; Cren, T.; Cherkez, V.; Debontridder, F.; Pons, S.; Fokin, D.; Tringides, M. C.; Bozhko, S.; Ioffe, L. B.; Altshuler, B. L.; Roditchev, D. Remarkable effects of disorder on superconductivity of single atomic layers of lead on silicon. *Nat. Phys.* **2014**, *10*, 444−450.

(5) Peng, J.; Yu, Z.; Wu, J.; Zhou, Y.; Guo, Y.; Li, Z.; Zhao, J.; Wu, C.; Xie, Y. Disorder Enhanced Superconductivity toward TaS_2 Monolayer. *ACS Nano* **2018**, *12*, 9461−9466.

(6) Ji, H.; Liu, H.; Jiang, H.; Xie, X. C. Disorder effects on quantum transport and quantum phase transition in low-dimensional superconducting and topological systems. *Adv. Phys.: X* **2021**, *6*, No. 1884133.

(7) Liu, M.; Nam, H.; Kim, J.; Fiete, G. A.; Shih, C. K. Influence of Nanosize Hole Defects and their Geometric Arrangements on the Superfluid Density in Atomically Thin Single Crystals of Indium Superconductor. *Phys. Rev. Lett.* **2021**, *127*, No. 127003.

(8) Veblen, D. R.; Heaney, P. J.; Angel, R. J.; Finger, L. W.; Hazen, R. M.; Prewitt, C. T.; Ross, N. L.; Chu, C. W.; Hor, P. H.; Meng, R. L. Crystallography, chemistry and structural disorder in the new high- T c Bi-Ca-Sr-Cu-O superconductor. *Nature* **1988**, *332*, 334−337.

(9) Dias, R. P.; Yoo, C. S.; Struzhkin, V. V.; Kim, M.; Muramatsu, T.; Matsuoka, T.; Ohishi, Y.; Sinogeikin, S. Superconductivity in highly disordered dense carbon disulfide. *Proc. Natl. Acad. Sci. U.S.A.* **2013**, *110*, 11720−11724.

(10) Snider, E.; Dasenbrock-Gammon, N.; McBride, R.; Debessai, M.; Vindana, H.; Vencatasamy, K.; Lawler, K. V.; Salamat, A.; Dias, R. P. Room-temperature superconductivity in a carbonaceous sulfur hydride. *Nature* **2020**, *586*, 373−377.

(11) Zarifi, N.; Liu, H.; Tse, J. S. Structures of the metallic and superconducting high pressure phases of solid CS_2. *Sci. Rep.* **2015**, *5*, No. 10458.

(12) Petrović, A. P.; Ansermet, D.; Chernyshov, D.; Hoesch, M.; Salloum, D.; Gougeon, P.; Potel, M.; Boeri, L.; Panagopoulos, C. A disorder-enhanced quasi-one-dimensional superconductor. *Nat. Commun.* **2016**, *7*, No. 12262.

(13) Haim, A.; Stern, A. Benefits of Weak Disorder in One-Dimensional Topological Superconductors. *Phys. Rev. Lett.* **2019**, *122*, No. 126801.

(14) Graybeal, J. M.; Mankiewich, P. M.; Dynes, R. C.; Beasley, M. R. Apparent Destruction of Superconductivity in the Disordered One-Dimensional Limit. *Phys. Rev. Lett.* **1987**, *59*, 2697−2700.

(15) Lowe, A.; Kagalovsky, V.; Yurkevich, I. V. Disorder-enhanced superconductivity in a quasi-one-dimensional strongly correlated system. *Phys. Rev. Res.* **2021**, *3*, No. 033059.

(16) Merlo, F.; Fornasini, M. L. Crystal structure of the $R_{11}Hg_{45}$ compounds (R = La, Ce, Pr, Nd, Sm, Gd, U). *J. Less-Common Met.* **1979**, *64*, 221−231.

(17) Iandelli, A. Crystal Structure of the Compounds LaHg, CeHg, PrHg, and NdHg, 1951.

(18) Iandelli, A. The structure of some ternary intermetallic compounds of the rare earths. *J. Alloys Compd.* **1994**, *203*, 137−138.

(19) Tkachuk, A. V.; Mar, A. In search of the elusive amalgam $SrHg_8$: A mercury-rich intermetallic compound with augmented pentagonal prisms. *Dalton Trans.* **2010**, *39*, 7132−7135.

(20) Todorov, E.; Sevov, S. C. Synthesis and structure of the alkali-metal amalgams A_3Hg_{20} (A = Rb, Cs), K_3Hg_{11}, Cs_5Hg_{19}, and A_7Hg_{31} (A = K, Rb). *J. Solid State Chem.* **2000**, *149*, 419−427.

(21) Biehl, E.; Deiseroth, H. J. Rb_5Hg_{19}: Eine neue, geordnete defektvariante des BaAl4-strukturtyps. *Z. Anorg. Allg. Chem.* **1999**, *625*, 389−394.

(22) Tkachuk, A. V.; Mar, A. $Li_6A_{17}Hg_9$ (A=Ca, Sr, Yb): Intermetallic compounds of mercury with a zeolite-like topology of cubic networks. *Chem. - Eur. J.* **2009**, *15*, 10348−10351.

(23) Sappl, J.; Freund, R.; Hoch, C. Stuck in our teeth? Crystal structure of a new copper amalgam, Cu_3Hg. *Crystals* **2017**, *7*, No. 352.

(24) Tambornino, F.; Hoch, C. The simplest representative of a complex series: The Hg-rich amalgam $Yb_{11}Hg_{54}$. *Z. Kristallogr. - Cryst. Mater.* **2017**, *232*, 557−565.

(25) Berndt, A. F. The crystal structure of Ce_5Hg_{21}. *J. Less-Common Met.* **1967**, *13*, 366−368.
(26) Hoch, C.; Simon, A. $Na_{11}Hg_{52}$: Complexity in a Polar Metal. *Angew. Chem., Int. Ed.* **2012**, *51*, 3262−3265.
(27) Svanidze, E.; Amon, A.; Borth, R.; Prots, Y.; Schmidt, M.; Nicklas, M.; Leithe-Jasper, A.; Grin, Y. Empirical way for finding new uranium-based heavy-fermion materials. *Phys. Rev. B* **2019**, *99*, No. 220403.
(28) Tambornino, F.; Hoch, C. The Mercury-richest Europium Amalgam $Eu_{10}Hg_{55}$. *Z. Anorg. Allg. Chem.* **2015**, *641*, 537−542.
(29) Tambornino, F.; Hoch, C. Bad metal behaviour in the new Hg-rich amalgam KHg_6 with polar metallic bonding. *J. Alloys Compd.* **2015**, *618*, 299−304.
(30) Hoch, C.; Simon, A. Cs_2Hg_{27}, das quecksilberreichste Amalgam − ein naher Verwandter der Bergman-Phasen. *Z. Anorg. Allg. Chem.* **2008**, *634*, 853−856.
(31) Tkachuk, A. V.; Mar, A. Alkaline-earth metal mercury intermetallics $A_{11-x}Hg_{54+x}$ (A = Ca, Sr). *Inorg. Chem.* **2008**, *47*, 1313−1318.
(32) Orlando, M. T. D.; Passos, C. A. C.; Passamai, J. L.; Medeiros, E. F.; Orlando, C. G. P.; Sampaio, R. V.; Correa, H. S. P.; de Melo, F. C. L.; Martinez, L. G.; Rossi, J. L. Distortion of ReO_6 octahedron in the $Hg_{0.82}Re_{0.18}Ba_2Ca_2Cu_3O_{8+d}$ superconductor. *Phys. C* **2006**, *434*, 53−61.
(33) Klein, W.; Kremer, R. K.; Jansen, M. $Hg_2Ru_2O_7$, a new pyrochlore showing a metal-insulator transition. *J. Mater. Chem.* **2007**, *17*, 1356−1360.
(34) van Duijn, J.; Ruiz-Bustos, R.; Daoud-Aladine, A. Kagome-like lattice distortion in the pyrochlore material $Hg_2Ru_2O_7$. *Phys. Rev. B* **2012**, *86*, No. 214111.
(35) Mostafa, M. F.; Hassen, A.; Kunkel, H. P. Irreversibility line of an Ag-doped Hg-based superconductor. *Supercond. Sci. Technol.* **2010**, *23*, No. 085010.
(36) Sakamoto, N.; Akune, T.; Ruppert, U. AC susceptibility studies of inter-grains in Hg-1223 superconductors. *J. Phys.: Conf. Ser.* **2008**, *97*, No. 012067.
(37) Kubo, M.; Akune, T.; Sakamoto, N.; Khan, H. R.; Lüders, K. Superconductivity of Ag-added composites of Hg-1223 grained Bean model. *Phys. C* **2007**, *463*−*465*, 478−481.
(38) Passos, C. A. C.; Orlando, M. T. D.; Oliveira, F. D. C.; da Cruz, P. C. M.; Passamai, J. L.; Orlando, C. G. P.; Elói, N. A.; Correa, H. P. S.; Martinez, L. G. Effects of oxygen content on the properties of the $Hg_{0.82}Re_{0.18}Ba_2Ca_2Cu_3O_{8+d}$ superconductor. *Supercond. Sci. Technol.* **2002**, *15*, 1177−1183.
(39) Knížek, K.; Veverka, M.; Hadová, E.; Hejtmánek, J.; Sedmidubský, D.; Pollert, E. Synthesis of $HgBa_2CuO_{4+\delta}$ by sol-gel method under controlled oxygen pressure; electron and thermal transport properties. *Phys. C* **1998**, *302*, 290−298.
(40) Yu, Y.; Zeng, Z. Y.; Xu, X. N.; Shao, H. M.; Qin, M. J.; Jin, X.; Yao, X. X.; Rong, X. S.; Ying, B.; Zhao, Z. X. Temperature dependence of the critical current determined from magnetic relaxation in $HgBa_2Ca_2Cu_3O_{8+\delta}$. *Phys. C* **1998**, *298*, 240−246.
(41) Karpinski, J.; Schwer, H.; Mangelschots, I.; Conder, K.; Morawski, A.; Lada, T.; Paszewin, A. Crystals of Hg superconductors. *Nature* **1994**, *371*, No. 661.
(42) Schwer, H.; Karpinski, J.; Conder, K.; Lesne, L.; Rossel, C.; Morawski, A.; Lada, T.; Paszewin, A. X-ray single-crystal structure refinement of the 129 K superconductor $Hg_xPb_{1-x}Ba_2Ca_3Cu_4O_{10+\delta}$. *Phys. C* **1995**, *243*, 10−18.
(43) Lin, C. T.; Yan, Y.; Peters, K.; Schönherr, E.; Cardona, M. Flux growth of $Hg_{1-x}Re_xBa_2Ca_{n-1}Cu_nO_{2n+2+\delta}$ single crystals by self-atmosphere. *Phys. C* **1998**, *300*, 141−150.
(44) Gatt, R.; Olsson, E.; Morawski, A.; Lada, T.; Paszewin, A.; Bryntse, I.; Grishin, A. M.; Eeltsev, Y.; Berastegui, P.; Johansson, L. G. Hg-1212 and Hg-1223 single crystals: Synthesis and characterisation. *Phys. C* **1997**, *276*, 270−276.
(45) Karpinski, J.20 Years High Pressure Materials Synthesis Group Activity after Discovery of High-T_c Superconductors. In *High T_c Superconductors and Related Transition Metal Oxides*; Springer: Berlin Heidelberg, 2007; pp 167−175.
(46) Karpinski, J. High pressure in the synthesis and crystal growth of superconductors and III−N semiconductors. *Philos. Mag.* **2012**, *92*, 2662−2685.
(47) Extremera, A. On the surface magnetization in superconducting $NaHg_4$. *J. Less-Common Met.* **1987**, *134*, 195−200.
(48) Dumett Torres, D.; Banerjee, P.; Pamidighantam, S.; Jain, P. K. A Non-Natural Wurtzite Polymorph of HgSe: A Potential 3D Topological Insulator. *Chem. Mater.* **2017**, *29*, 6356−6366.
(49) Ruan, J.; Jian, S. K.; Yao, H.; Zhang, H.; Zhang, S. C.; Xing, D. Symmetry-protected ideal Weyl semimetal in HgTe-class materials. *Nat. Commun.* **2016**, *7*, No. 11136.
(50) Yan, B.; Felser, C. Topological materials: Weyl semimetals. *Annu. Rev. Condens. Matter Phys.* **2017**, *8*, 337−354.
(51) Ornes, S. Topological insulators promise computing advances, insights into matter itself. *Proc. Natl. Acad. Sci. U.S.A.* **2016**, *113*, 10223−10224.
(52) Li, L.; Li, Y.; Jin, Y.; Huang, H.; Chen, B.; Xu, X.; Dai, J.; Zhang, L.; Yang, X.; Zhai, H.; Cao, G.; Xu, Z. Coexistence of superconductivity and ferromagnetism in $Sr_{0.5}Ce_{0.5}FBiS_2$. *Phys. Rev. B* **2015**, *91*, No. 014508.
(53) Vergniory, M. G.; Elcoro, L.; Felser, C.; Regnault, N.; Bernevig, B. A.; Wang, Z. A complete catalogue of high-quality topological materials. *Nature* **2019**, *566*, 480−485.
(54) Autieri, C.; Śliwa, C.; Islam, R.; Cuono, G.; Dietl, T. Momentum-resolved spin splitting in Mn-doped trivial CdTe and topological HgTe semiconductors. *Phys. Rev. B* **2021**, *103*, No. 115209.
(55) Extremera, A. The magnetic behaviour of $NaHg_4$ peritectic. *Phys. Status Solidi (a)* **1988**, *105*, 281−284.
(56) Extremera, A. Excess molar volume and m/m* effects in the magnetic behaviour of liquid HgNa alloys. *J. Phys.: Condens. Matter* **1991**, *3*, 3663−3666.
(57) Kim, J. S.; Stewart, G. R. UHg 3: A heavy-fermion antiferromagnet similar to U_2Zn_{17} and UCd_{11}, RAPID Commun. *Phys. Rev. B* **2014**, *89*, No. 41103.
(58) Stock, C.; Rodriguez-Rivera, J. A.; Schmalzl, K.; Demmel, F.; Singh, D. K.; Ronning, F.; Thompson, J. D.; Bauer, E. D. From Ising Resonant Fluctuations to Static Uniaxial Order in Antiferromagnetic and Weakly Superconducting $CeCo(In_{1-x}Hg_x)_5$(x = 0.01). *Phys. Rev. Lett.* **2018**, *121*, No. 037003.
(59) Bao, W.; Gasparovic, Y. C.; Lynn, J. W.; Ronning, F.; Bauer, E. D.; Thompson, J. D.; Fisk, Z. Commensurate magnetic structure of $CeRhIn_{4.85}Hg_{0.15}$. *Phys. Rev. B* **2009**, *79*, No. 092415.
(60) Tang, J.; Gschneidner, K. A. Antiferromagnetic ordering in $CeHg_3$. *Phys. B* **1997**, *230*−*232*, 186−188.
(61) Morachevskii, A. G. Liquid alloys of the mercury-sodium system: Thermodynamics, structure, and applications. *Russ. J. Appl. Chem.* **2014**, *87*, 837−852.
(62) Morawski, A.; Paszewin, A.; Lada, T.; Marciniak, H.; et al. Mercury superconductors crystal growth under high pressure and high temperature influenced by crucible composition. *IEEE Trans. Appl. Supercond.* **1997**, *7*, 1903−1906.
(63) Loret, B.; Forget, A.; Moussy, J. B.; Poissonnet, S.; Bonnaillie, P.; Collin, G.; Thuéry, P.; Sacuto, A.; Colson, D. Crystal Growth and Characterization of $HgBa_2Ca_2Cu_3O_{8+\delta}$ Superconductors with the Highest Critical Temperature at Ambient Pressure. *Inorg. Chem.* **2017**, *56*, 9396−9399.
(64) Tambornino, F.; Sappl, J.; Pultar, F.; Cong, T. M.; Hübner, S.; Giftthaler, T.; Hoch, C. Electrocrystallization: A Synthetic Method for Intermetallic Phases with Polar Metal-Metal Bonding. *Inorg. Chem.* **2016**, *55*, 11551−11559.
(65) Bruzzone, G.; Merlo, F. The lanthanum-mercury system. *J. Less-Common Met.* **1976**, *44*, 259−265.
(66) Leithe-Jasper, A.; Borrmann, H.; Hönle, W.Das Laboratorium hoher Schutzklasse (LHS), MPI CPfS: Dresden, 2005. http://www2.cpfs.mpg.de/web/docs/scientreport/report2006_data/SR%20pages24-27.pdf?cpfs_id=000469 (accessed 2022-08-31).

https://doi.org/10.1021/acs.inorgchem.2c01987
Inorg. Chem. 2022, 61, 15444−15451

(67) Rundle, R. E.; Wilson, A. S. The structures of some metal compounds of uranium. *Acta Crystallogr.* **1949**, *2*, 148−150.
(68) Frost, B. R. T. The system uranium-mercury. *Vacuum* **1954**, *4*, 368−369.
(69) Cabane, G. Constitution of uranium and thorium alloys. *J. Nucl. Mater.* **1960**, *2*, No. 94.
(70) Guminski, C. The Hg-U (mercury-uranium) system. *J. Phase Equilib.* **2003**, *24*, 461−468.
(71) *STOE Powder Software, Software, WinXPow (version 2), Darmstadt, STOE and Cie GmbH*, 2001.
(72) Akselrud, L.; Grin, Y. WinCSD: Software package for crystallographic calculations (Version 4). *J. Appl. Crystallogr.* **2014**, *47*, 803−805.
(73) Donohue, J.*Structures of the Elements*; Wiley, 1974.

NOTE ADDED AFTER ASAP PUBLICATION

This paper was published on September 2, 2022. Dimensions were corrected in the caption for Figure 1, and the paper was reposted on September 21, 2022.

https://doi.org/10.1021/acs.inorgchem.2c01987
Inorg. Chem. 2022, 61, 15444−15451